

Document downloaded from:

<http://hdl.handle.net/10251/181772>

This paper must be cited as:

Cerqueira, A.; Araújo-Gomes, N.; Zhang, Y.; Van Den Beucken, JJJP.; Martínez-Ramos, C.; Ozturan, S.; Izquierdo, R.... (2021). Evaluation of the inflammatory responses to sol-gel coatings with distinct biocompatibility levels. *Journal of Biomedical Materials Research Part A*. 109(9):1539-1548. <https://doi.org/10.1002/jbm.a.37149>



The final publication is available at

<https://doi.org/10.1002/jbm.a.37149>

Copyright John Wiley & Sons

Additional Information

1 **Title Page**

2

3 **Evaluation of the inflammatory responses to sol-gel coatings with distinct**  
4 **biocompatibility levels**

5

6 **Authors**

7 A. Cerqueira<sup>1\*</sup>, N. Araújo-Gomes<sup>2\*</sup>, Y. Zhang<sup>3, 4</sup>, J.J.J.P van den Beucken<sup>3</sup>, C. Martínez-  
8 Ramos<sup>5</sup>, S. Ozturan<sup>6</sup>, R. Izquierdo<sup>1</sup>, M. Muriach<sup>7</sup>, R. Romero-Cano<sup>7</sup>, P. Baliño<sup>7</sup>, F. Romero-  
9 Gavilán<sup>1#</sup>

10

11 <sup>1</sup>Department of Industrial Systems Engineering and Design, Universitat Jaume I, Av. Vicent  
12 Sos Baynat s/n, 12071 Castellón de la Plana, Spain

13 <sup>2</sup>Department of Developmental Bioengineering, University of Twente, Faculty of Science and  
14 Technology, 7522LW, Enschede, The Netherlands

15 <sup>3</sup>Dentistry – Regenerative Biomaterials, PO Box 9101, 6500 HB, Radboudumc, Nijmegen,  
16 The Netherlands

17 <sup>4</sup>School of Medicine, Shenzhen University, Shenzhen, Guangdong Province, 518037, China

18 <sup>5</sup>Center for Biomaterials and Tissue Engineering, Universitat Politècnica de Valencia, Camino  
19 de Vera, s/n 46022 Valencia, Spain

20 <sup>6</sup>Department of Periodontology, Faculty of Dentistry, Istanbul Medeniyet University,  
21 Istanbul, Turkey

22 <sup>7</sup>Unidad Pre-Departmental de Medicina, Universitat Jaume I, Av. Vicent Sos Baynat s/n,  
23 12071 Castellón de la Plana, Spain

24

25 \* Co-authorship

26

27 #Corresponding author:

28 Francisco Romero-Gavilán

29 Department of Industrial Systems Engineering and Design – Universitat Jaume I

30 Campus del Riu Sec, Avda. Vicent Sos Baynat s/n

31 12071 – Castelló de la Plana (Espanya)

32 E-mail: gavilan@uji.es

33

34 **Title:** Evaluation of the inflammatory responses to sol-gel coatings with distinct  
35 biocompatibility levels

36 **Abstract:** The immune system plays a crucial role in determining the implantation outcome,  
37 and macrophages are in the frontline of the inflammatory processes. Further, cellular  
38 oxidative stress resulting from the material recognition can influence how cell responses  
39 develop. Considering this, the aim of this study was to study oxidative stress and  
40 macrophages phenotypes in response to sol-gel materials with distinct *in vivo* outcomes. Four  
41 materials were selected (70M30T and 35M35G30T, with high biocompatibility, and 50M50G  
42 and 50V50G, with low biocompatibility). Gene expression, immunocytochemistry and  
43 cytokine secretion profiles for M1 and M2 markers were determined. Moreover, oxidative  
44 stress markers were studied. Immunocytochemistry and ELISA showed that 50M50G and  
45 50V50G lead to a higher differentiation to M1 phenotype, while 70M30T and 35M35G30T  
46 promoted M2 differentiation. In oxidative stress, no differences were found. These results  
47 show that the balance between M1 and M2, more than individual quantification of each  
48 phenotype, determines a biomaterial outcome.

49 **Keywords:** Inflammation; macrophage plasticity; biomaterials; oxidative markers; implants

## 50 **1. Introduction**

51 Biocompatibility describes the appropriate biological requirements of biomaterials for  
52 medical application as well as the ability of said materials to perform with an host response in  
53 a specific application <sup>(1)</sup>. It is determined by the coordination of the host homeostatic  
54 mechanisms, which are disturbed upon implantation, and the consequent immune response to  
55 injury <sup>(2)</sup>. The coordinated activation, type and action of highly specialized immune cells  
56 depends of the nature and site of the wound/damage <sup>(3)</sup>. Macrophages represent the first line  
57 of defense on the innate immunity, being most known by their phagocytic capabilities.

58 Besides their major effector function of eliminating and inactivating pathogens, these cells  
59 boost properties such as the clearance of apoptotic cells throughout the lifespan of an  
60 organism, homeostasis and activation of tissue repair processes <sup>(4)</sup>. Macrophages have the  
61 capability to enter into distinct tissues, modulate and differentiate into specialized phenotypes  
62 according to microenvironmental cues, stimuli from growth factors, cytokines, and  
63 chemokines present in biological fluids (*e.g.* blood). In the case of implanted biomaterials,  
64 these events are part of a whole process that could culminate in a foreign body reaction (FBR)  
65 to the material <sup>(5)</sup>. Once activated, macrophages can exhibit a spectrum of polarization states  
66 depending on their functional nature, adopting a pro-inflammatory phenotype (M1) or an anti-  
67 inflammatory phenotype (M2), with distinct surface markers and/or different gene expression  
68 profiles. When a biomaterial is implanted into the organism, this cascade of events is  
69 triggered, allowing the direct and initial migration of M1 macrophages toward the  
70 implantation site, provoking the necessary inflammatory response <sup>(6)</sup>, which is characterized  
71 by the secretion of pro-inflammatory cytokines and chemokines, such as tumor necrosis factor  
72  $\alpha$  (TNF- $\alpha$ ) and interleukin 1- $\beta$  (IL-1 $\beta$ ) <sup>(7)</sup>. The prolonged presence of this phenotype can lead  
73 to a state of chronic inflammation, ultimately leading to implant rejection <sup>(8)</sup>. The anti-  
74 inflammatory M2 macrophages establish themselves upon signals released by basophils,  
75 including cytokines like interleukin-10 (IL-10) and interleukin-4 (IL-4) <sup>(9)</sup>. This anti-  
76 inflammatory state is distinguishable by its role on immunoregulation, matrix deposition and  
77 tissue remodeling processes <sup>(7)</sup>. The increase of M2 subsets in the biomaterial surrounding  
78 environment, towards a positive value of M2:M1 ratio, has been suggested as the key to a  
79 positive outcome of the implanted material <sup>(10)</sup>. However, the greater presence of M2  
80 macrophages could increase of foreign body giant cells (FBGC) *in situ*, when its  
81 predominance is too prolonged <sup>(5)</sup>. Hence, this ratio as a marker for biocompatibility must be  
82 carefully approached.

83 Oxidative stress derives as a consequence of the surgical creation of a wound and  
84 implantation, being influenced by the material properties, the degree of initial inflammation  
85 and the immediate stress resulting from the procedure, occurring at all stages of the response  
86 to a biomaterial. The resulting reactive oxygen species (ROS), reactive nitrogen species  
87 (RNS) and lipid peroxidation subproducts (*e.g.* malondialdehyde – MDA) act as chemo-  
88 attractants and signaling molecules during healing, and are often associated with phenotypic  
89 shifts of immune cells and modulation of cell response to a determined material <sup>(11)</sup>. Redox  
90 interactions are responsible for stabilizing these oxidation products and glutathione (GSH),  
91 synthesized from glycine, cysteine, and glutamic acid, is the most important redox-regulating  
92 thiol, acting as a substrate of glutathione peroxidase (GPx) <sup>(12)</sup>. The antioxidant function of  
93 GSH is due to the oxidation of the sulfhydryl group (-SH), and the ratio between glutathione  
94 disulfide (GSSH) and GSH is an indicator of the cellular redox potential <sup>(12)</sup>. Superoxide  
95 generation, namely hydrogen peroxide, is typically increased and associated to the M1  
96 macrophage phenotype, due to its phagocytic/microbiocidal activity, which depends on the  
97 synthesis of ROS and RNS. Moreover, as M2 phenotypes are usually described as being  
98 angiogenic, anti-oxidant and dependent on oxidative phosphorylation, apparent oxidative  
99 metabolic differences are reported for these immune cell subpopulations <sup>(13)</sup>. Upon  
100 implantation on a living organism, the blood is the first organic fluid in contact with the  
101 implant, leading to protein adsorption by the surface whose type, composition, quantity and  
102 conformation might impair the final outcome <sup>(14)</sup>. This process is dependent on the  
103 physicochemical characteristics of the surface of the material and can ultimately modulate  
104 macrophage and monocyte activation and migration to the implantation site <sup>(15)</sup>. In previous  
105 studies <sup>(16)</sup>, we showed that a greater deposition of complement proteins onto a biomaterial is  
106 intrinsically correlated with their biocompatibility in a living host. The oxidative stress in  
107 response to the implantation process and the material itself might also directly impair the

108 immune cellular response/differentiation and ultimately affect the implant outcome.

109 Following this premise, this experimental work focuses on the study of the  
110 polarization/plasticity of activated macrophages to previously described sol-gel materials with  
111 distinct biocompatibility reactions *in vivo* and the correlation of between the predominance of  
112 a determined macrophage phenotype with the oxidative stress responses.

## 113 **2. Materials and methods**

### 114 **2.1. Material selection, synthesis, and preparation**

115 Sol-gel technology was employed to synthesize four different materials using  
116 methyltrimethoxysilane (MTMS), 3-glycidoxypropyl-trimethoxysilane (GPTMS), tetraethyl  
117 orthosilicate (TEOS) and triethoxyvinylsilane (VTES) precursors in the proportions shown in  
118 Table 1. These materials, designed in previous works, were selected due to their distinct  
119 biocompatibility outcomes *in vivo* <sup>(16)-(18)</sup>. For their synthesis, the corresponding alkoxy silane  
120 amounts were diluted with 2-propanol (50 % vol) and hydrolyzed adding the stoichiometric  
121 amount of acidified aqueous solution (0.1 M HNO<sub>3</sub>). All the employed reagents were  
122 purchased from Sigma-Aldrich (Merck KGaA, Darmstadt, Germany). The sol-gel  
123 preparations were left stirring for 1 h and resting for another 1 h. The coatings were prepared  
124 immediately after this resting. For that, grade- 4 Ti discs (12 mm diameter, 1 mm thick;  
125 Ilerimplant-GMI S.L., Lleida, Spain) were employed as substrate for the coatings. Bare discs  
126 were superficially pre-treated with a sandblasting and acid-etching treatment (SAE)  
127 previously described <sup>(19)</sup>. Then, the sol-gel solutions were applied as coatings using a KSV  
128 DC dip-coater (Biolin Scientific, Stockholm, Sweden). Discs were submerged into the  
129 corresponding sol-gel (60 cm min<sup>-1</sup>-speed) and kept immersed in it for one minute. Then, the  
130 samples were taken out at 100 cm min<sup>-1</sup>. Finally, heat treatments at 80 °C to 70M30T and  
131 35M35G30T, and at 140°C to 50M50G and 50V50G materials were carried out for 2 h.

132 **2.2. *In vitro* assays**

133 **2.2.1. Cell culture**

134 For the distinct experiments, mouse murine macrophage cells (RAW 264.7) were cultured on  
135 the discs in 48-well NUNC plates (Thermo Fisher Scientific, NY, USA) at 37 °C in a  
136 humidified (95 %) CO<sub>2</sub> incubator using as culture medium Dulbecco's Modified Eagle  
137 Medium (DMEM; Gibco, Thermo Fisher Scientific) with 10 % of fetal bovine serum (FBS;  
138 Gibco) and 1 % of penicillin/streptomycin (Gibco).

139 **2.2.2. Cell fixation for SEM imaging**

140 After 72 h of incubation, samples were washed once with PB 0.1 M and fixed with 3.5 %  
141 glutaraldehyde for 45 minutes, at 37 °C, in the dark. After washing twice with PB 0.1 M, the  
142 preparations were incubated with 2 % osmium for 1 h in the dark. Afterwards, samples were  
143 washed with dH<sub>2</sub>O to eliminate any osmium residues and a chain with crescent concentrations  
144 of ethanol was performed for dehydration. The critical point drying was made through  
145 incubation with hexamethyldisilazane (HDMS; Sigma-Aldrich). Next, samples were  
146 examined in a field emission scanning electron microscope (FESEM; ULTRA 55, ZEISS  
147 Oxford Instruments) at 2kV of voltage.

148 **2.2.3. Immunocytochemistry double staining**

149 After 24 and 72 h, samples were fixed in 4 % paraformaldehyde for 10 min (Sigma-Aldrich)  
150 and washed five times in 1x PBS. The samples were blocked in 1x PBS containing 0.5 %  
151 BSA and 1 % Triton X-100 (Sigma-Aldrich). They were incubated with donkey anti-mouse  
152 CD206 primary antibody (Abcam, Cambridge, UK) diluted 1:250 in PBS containing 0.5 %  
153 BSA and 0.5 % Tween-20 (Sigma-Aldrich), overnight at 4°C. The discs were then washed  
154 five times in 1x PBS and incubated with a mixture of secondary antibodies composed of Goat  
155 anti-Donkey Biotin (Jackson ImmunoResearch Europe, Ltd., Cambridgeshire, UK) diluted

156 1:500 and Streptavidin Alexa Fluor 647 (Thermo Fisher Scientific) diluted 1:500 for 1 h at  
157 room temperature. Cells were washed five times with wash buffer (1x PBS with 0.5 % Triton  
158 X-100) and incubated with the primary antibody IL7-R (Santa Cruz Biotechnology, Dallas,  
159 TX, USA) at 4 °C overnight. After five washes with wash buffer, the discs were incubated  
160 with the secondary antibody Goat anti-Rabbit Alexa Fluor 488 (Thermo Fisher Scientific) for  
161 1 h at room temperature. After the next five washes with wash buffer, the discs were  
162 incubated with DAPI (Roche, Basel, Switzerland) for another hour to stain the cell nuclei.

163 The discs were then removed from the wells, mounted on coverslipped slides with mounting  
164 medium to prevent the sample from drying out (4.8 % poly(vinyl alcohol-co-vinyl acetate), 12  
165 % glycerol, 0.2 M Tris-HCl, 0.02 % sodium azide) and stored at 4°C until the fluorescence  
166 microscopy analysis (Keyence International, Mechelen, Belgium).

#### 167 **2.2.4. RNA extraction, cDNA synthesis and quantitative real-time PCR measurements**

168 After 24 and 72 h, total RNA was extracted using TRIzol (1 M guanidine thiocyanate, 1 M  
169 ammonium thiocyanate, 3 M sodium acetate, 5 % glycerol, 38 % aquaphenol). To each  
170 sample 300 µL of TRIzol were added followed by an incubation at room temperature. After  
171 centrifugation (5 min, 13000 rpm, 4 °C), 200 µL of chloroform were added to the supernatant,  
172 and the samples were centrifuged (5 min, 13000 rpm, 4 °C). The aqueous layer was mixed  
173 with 550 µL of isopropanol and kept at room temperature for 10 min. Samples were  
174 centrifuged (15 min, 13000 rpm, 4 °C), and washed twice with 0.5 mL of 70 % ethanol. The  
175 resulting pellet was dissolved in 30 µL of RNase free water. RNA concentration, integrity,  
176 and quality were measured using NanoVue® Plus Spectrophotometer (GE Healthcare Life  
177 Sciences, Little Chalfont, UK). Approximately 1 µg of total RNA was converted into cDNA  
178 using PrimeScript RT Reagent Kit (Perfect Real Time; TAKARA Bio Inc., Shiga, Japan) and  
179 the reaction was conducted with the following conditions: 37 °C for 15 min, 85 °C for 5 secs  
180 and a final hold at 4°C. The resulting cDNA quality and quantity was measured using a



181 NanoVue® Plus Spectrophotometer (GE Healthcare Life Sciences), then diluted in DNase-  
182 free water to a concentration suitable for reliable qRT-PCR analysis and stored at -20 °C.

183 To evaluate the effects of the materials on the inflammatory responses, genes corresponding  
184 to pro and anti-inflammatory phenotypes were selected (Table 2). *GADPH* was used as a  
185 housekeeping gene. Primers were designed using DNA sequences for these genes available  
186 from NCBI (<https://www.ncbi.nlm.nih.gov/nucleotide>), employing PRIMER3plus software tool  
187 (<http://www.bioinformatics.nl/cgi-bin/primer3plus/primer3plus.cgi>) and purchased to Thermo  
188 Fischer Scientific. Quantitative real-time PCR (qRT-PCR) were carried out in 96-well plates  
189 (Applied Biosystems®, Thermo Fisher Scientific) and individual reactions contained 1 µL of  
190 cDNA, 0.2 µL of specific primers (forward and reverse at 10 µM L<sup>-1</sup>) and 5 µL of SYBR  
191 Premix Ex Taq (Tli RNase H Plus; TAKARA, Bio Inc., Shiga, Japan) in a final volume of 10  
192 µL, and were carried out in a StepOne Plus™ Real-Time PCR System (Applied  
193 Biosystems®). The cycling parameters were an initial denaturation step (95°C, 30 s) followed  
194 by 95 °C for 5 s and 60 °C for 34 s, for 40 cycles. The final melt curve stage comprised a  
195 cycle at 95 °C for 15 s and at 60 °C, for 60 s. Fold changes were calculated using the 2<sup>-ΔΔCt</sup>  
196 method and the data was normalized in relation to the blank wells (without any material).

#### 197 **2.2.5. Cytokine quantification by ELISA**

198 To measure secreted cytokines (TNF-α, IL-1β, TGF-β and IL-10), the cell culture  
199 supernatants used for immunocytochemistry were collected and frozen until further analysis.  
200 The concentration of these cytokines was determined using an ELISA (Invitrogen, Thermo  
201 Fisher Scientific) kit and according to the manufacturer's instructions.

#### 202 **2.2.7. Oxidative stress**

203 After 24 and 72 h, cells were washed three times with PBS and incubated at 4 °C for 10 min  
204 in lysis buffer (0.2 % Triton X-100, 10 mM Tris-HCl, pH 7.2). Glutamic acid, glutathione

205 (GSH) and glutathione disulfide (GSSG) concentrations were quantified chromatographically  
206 using the method proposed by Reed <sup>(20)</sup>. Shortly, this method is based in the reaction of the  
207 Sanger Reactant (1-fluoro-2,4-dinitrobenzene) with amino groups and iodoacetic acid to  
208 block free thiol groups. Samples were measured after derivatization using a high-performance  
209 liquid chromatographic system equipped with a diode array detector. Glutathione peroxidase  
210 activity (GPx) was determined by the disappearance of NADPH monitored at 340 nm as  
211 proposed Lawrence *et al.* <sup>(21)</sup>. Briefly, a solution containing 50  $\mu\text{L}$  of samples, 550  $\mu\text{L}$  of  
212 potassium phosphate buffer 0.1 M pH 7.0, EDTA 1 mM and  $\text{NaN}_3$  1 mM was mixed with 100  
213  $\mu\text{L}$  GSH disulfide reductase ( $0.24 \text{ U mL}^{-1}$ ), 100  $\mu\text{L}$  glutathione reduced 1 mM and 100  $\mu\text{L}$   
214 NADPH 0.15 mM. The resulting solution was incubated for 3 min at 37 °C. Then, 100  $\mu\text{L}$  of  
215 hydrogen peroxide 1.5 mM were added to start the reaction. Glutathione reductase activity  
216 was determined using the method proposed by Smith and *et al.* <sup>(22)</sup>. The method consists in  
217 monitoring spectroscopically the 2-nitrobenzoic acid formation. This is formed as subproduct  
218 of the GR catalyzed reduction of GSSG to GSH in presence of 5,5'-dithiobis(2-nitrobenzoic  
219 acid) (DTNB). The GSSG reduction was started by adding 25  $\mu\text{L}$  of sample to a solution  
220 containing 450  $\mu\text{L}$  0.2 M phosphate buffer pH7.5 and 250  $\mu\text{L}$  of DTNB 3 mM prepared in 10  
221 mM phosphate buffer, 50  $\mu\text{L}$  of 2 mM NADPH and 50  $\mu\text{L}$  of 10 mM EDTA. Total volume  
222 was adjusted to 1 mL using ultrapure water and the wavelength set at 412 nm. MDA  
223 concentration was determined chromatographically using an HPLC system using Richard *et*  
224 *al.* proposed method <sup>(23)</sup> with modifications introduced by Romero *et al.* <sup>(24)</sup>. Sample  
225 preparation consisted in mixing samples (100  $\mu\text{L}$ ) with 0.75 mL of thiobarbituric acid with  
226 0.37 % and perchloric acid 6.4 % (2:1, v/v) and heated to 95 °C for an hour. Then, pH was  
227 adjusted to 6 and precipitates removed by centrifugation (10000 rpm, 1 min). Separation was  
228 carried out in a HPLC system equipped with a C18 250x4.6 mm 5  $\mu\text{m}$  chromatographic  
229 column using an isocratic separation. Flow was set at  $1 \text{ mL min}^{-1}$  and fluorescence detector

230 was set to 527 nm for excitation and 532 nm for emission. Mobile phase consisted in 50 mM  
231 phosphate buffer (pH 6.0): methanol (58:42, v/v) and 1,1,3,3-tetramethoxypropane was used  
232 as standard solution. All standards and mobile phases were prepared daily. Protein levels were  
233 determined from cell culture lysates using a Pierce™ BCA Protein Assay Kit (Thermo Fisher  
234 Scientific) and used to normalize oxidative stress values.

### 235 **2.3. Statistical analysis**

236 Based on the normal distribution and equal variance assumption test, the data were analyzed  
237 via one-way analysis of variance (ANOVA) with Newman-Keuls post hoc test and expressed  
238 as mean ± standard deviation (SD). Statistical analysis was performed using GraphPad Prism  
239 5.04 software (GraphPad Software Inc., La Jolla, CA, USA). The asterisk (\*) indicates  
240 statistically significant ( $p \leq 0.05$ ) differences between the four materials.

## 241 **3. Results**

### 242 **3.1. Morphological analysis**

243 To evaluate cellular morphology, macrophages seeded on the distinct materials were studied  
244 with SEM. The obtained images of cell spreading revealed that macrophages seeded for 72 h  
245 on 70M30T and 35M35G30T treatment acquired an elongated morphology (Fig. 1a', 1b').  
246 When seeded on 50M50G and 50V50G, macrophages adhered and spread to a typical  
247 rounded shape (Fig. 1c', 1d').

### 248 **3.2. Immunocytochemistry double staining**

249 To evaluate the expression of markers associated with M1 and M2 phenotypes,  
250 immunocytochemistry was performed. IL7-R, an M1-phenotype marker, showed significant  
251 increased fluorescence of the macrophage cultures on the 50V50G and 50M50G when  
252 compared to the other two materials (Fig. 2). No differences were observed on the CD206  
253 M2-marker fluorescence intensity.

### 254 **3.3. Gene expression analysis**

255 The expression of pro and anti-inflammatory markers by the RAW264.7 cells cultured onto  
256 the distinct materials is shown in Fig. 3. At 24h, the expression of TNF- $\alpha$  was significantly  
257 higher on 35M35G30T, generally decreasing at 72 h on all materials (Fig. 3a). On the other  
258 hand, IL1- $\beta$  expression peaked at 24 h and then decreased on all materials at 72h (Fig. 3b). No  
259 statistical differences were found for iNOS expression. Regarding anti-inflammatory markers,  
260 a significant increase of TGF- $\beta$  was observed for 50M50G at 24 h, but after 72 h no  
261 differences between materials were observed (Fig. 3d). The expression of IL-10 showed  
262 differences at 72 h with a significantly higher expression on 50V50G (Fig. 3e). The  
263 expression of EGR2 was significantly lower on 70M30T at 24 h compared to the other  
264 materials and decreased at 72 h (Fig. 3f).

### 265 **3.4. Cytokine quantification by ELISA**

266 To obtain data about inflammatory induction by these materials, secretion profiles of pro- and  
267 anti-inflammatory cytokines of RAW264.7 macrophages were assessed by ELISA (Fig. 4).  
268 RAW264.7 macrophages cultured on both 50M50G and 50V50G treatments showed a clear  
269 increased secretion of TNF- $\alpha$  at 24 h compared to those cultured on the 70M30T and  
270 35M35G30T materials. At 72 h, a marked high secretion of TNF- $\alpha$  for 50V50G was observed  
271 (Fig. 4a). Further, an increasing IL-10 release was observed on this material, with significance  
272 regarding the other materials (Fig. 4d). IL-1 $\beta$  was not detected until 72 h of culture, revealing  
273 no differences between materials.

### 274 **3.4. Oxidative stress**

275 Fig. 5 shows the macrophage oxidative stress markers (GSH, GSSG, GR, GPx and MDA)  
276 when cultured on sol-gel materials. No significant differences were found between materials  
277 at any time measured.

#### 278 4. Discussion

279 Implanting a biomaterial foreign body into a living host leads to immediate tissue damage and  
280 cell disruption resulting from the surgical procedure. The blood protein adsorption onto the  
281 surface of the material causes platelet degranulation, forming a provisional matrix that kick-  
282 starts tissue healing responses, inducing immune cell activation and migration <sup>(25)</sup>.

283 The composition, conformation and amount of the bound proteins is regulated their specific  
284 affinity and the biomaterial characteristics. Distinct biological responses can result by  
285 changing the surface and consequent protein adsorption; more specifically, emerging data  
286 suggest that the modulation of immune cells is directly driven by complement protein  
287 adsorption, affecting the *in vivo* biocompatibility of a material <sup>(26)</sup>. Immune cells interact  
288 closely with complement proteins inducing an initial inflammatory response that propagates  
289 depending on multiple factors and at implantation site activate and promote additional cellular  
290 events.

291 Macrophages present a high plasticity and can adopt a wide battery of phenotypes. The M1  
292 phenotype is characterized a pro-inflammatory response, the M2 phenotype presents anti-  
293 inflammatory characteristics. At initial stages of inflammatory responses, the M1 is the most  
294 prevalent but, with time, macrophages undergo a transition to the M2 phenotype. With a  
295 prolonged presence of a M1 phenotype on the local microenvironment surrounding the  
296 material, fibrous structures can be observed <sup>(5)</sup>. Thus, the hypothesis that a biomaterial leading  
297 to the formation of connective tissue structures possibly induces the differentiation of  
298 macrophages to a M1 phenotype arises. Previous work has shown that the materials with low  
299 biocompatibility (50M50G and 50V50G) lead to the formation of a fibrous capsule, while the  
300 materials with good biocompatibility (70M30T and 30M35G30T) did not present  
301 inflammatory structures. To understand these distinct *in vivo* responses, protein adsorption of

302 these two groups was compared. Results revealed higher adsorption of inflammatory-related  
303 proteins onto the surfaces related to biocompatibility problems <sup>(16)</sup>. The morphology acquired  
304 by macrophages when in contact with good biocompatible materials cells displayed an  
305 elongated form, with cytoplasmic projections on the apical edges, typical of M2-phenotype;  
306 on the other hand, on the materials with low biocompatibility, the cells adopted an round  
307 shape, with very frail extensions of the cytoplasm, characteristic of a M1 phenotype <sup>(27),(28)</sup>.  
308 Furthermore, higher quantities of TNF- $\alpha$  and IL-10 were secreted by the cells on the materials  
309 with low biocompatibility. This increased release of TNF- $\alpha$ , a M1 marker <sup>(29)</sup>, is observed for  
310 cells cultured on both 50M50G and 50V50G after short times of incubation (24 h). In  
311 addition, 50V50G showed this greater cytokine liberation even after 72 h, revealing a strong  
312 inflammatory potential with respect the other treatments. The upregulated secretion of IL-10  
313 on 50V50G, often considered a key M2 marker <sup>(29)</sup>, is dependent on the cell line <sup>(30)</sup>. In  
314 RAW264.7 cells exposed to LPS, IL-10 secretion is increased <sup>(31)</sup>. As described in Araújo-  
315 Gomes *et al.* <sup>(26)</sup>, GPTMS presents an epoxy ring in its structure that might mimic LPS.  
316 However, IL-10 secretion was not significantly higher on 50V50G. This might be due to the  
317 vinyl group of this formulation, as it was described to induce inflammation in hepatic murine  
318 cells <sup>(32)</sup>. These results point out that IL-10 biomarker could lead to incorrect conclusions in  
319 murine cells as it is dependent on the material chemistry. Interestingly, an overexpression of  
320 EGR2 was observed at 24 h on the materials with low biocompatibility. The EGR2 is  
321 described to have a specific role on RAW 264.7 macrophage plasticity. Specifically, EGR2 is  
322 described to be expressed by non-activated and M2 macrophages, whereas it is downregulated  
323 in M1 macrophages <sup>(33)</sup>, being modulated by the transcription factor CEBP $\beta$ . Moreover, this  
324 gene is described as being a “master controller” of inflammation by regulating B and T cell  
325 function to achieve immune homeostasis <sup>(34)</sup>. We hypothesize that the greater expression of  
326 this gene during the first 24 h on the GPTMS-based materials is due to the greater

327 inflammatory induction, to regulate and attenuate the inflammation caused by those specific  
328 materials. The immunocytochemistry supports the data obtained on by ELISA, disclosing  
329 higher tendency for the materials with low biocompatibility to induce the RAW 264.7 to  
330 differentiate toward a pro-inflammatory M1 phenotype. This distinct polarization points out to  
331 the increased inflammatory potential of the 50M50G and 50V50G coatings, which is coherent  
332 with the data obtained in a previous study and could explain the dissimilar biocompatibility  
333 associated with each of these materials <sup>(16)</sup>. However, it appears that 35M35G30T is also  
334 inducing an M1 phenotype compared to the 70M30T coating. This fact can be associated with  
335 the 35 % of GPTMS incorporated in the coating network. GPTMS-derived sol-gel materials  
336 showed an increased inflammatory potential, which in turn was directly correlated with a  
337 higher affinity of complement proteins to the material surface <sup>(26)</sup>. However, when comparing  
338 to 50M50G and 50V50G, we can conclude that this may be due to the lower percentage of the  
339 compound, therefore not compromising biocompatibility.

340 Although this data seems to identify clear and distinct cellular behavior when exposed to the  
341 materials, these differences were not be translated into the oxidative stress induction. Data  
342 obtained from oxidative stress measurements showed no differences between materials,  
343 suggesting once more that the inflammation is driven by the complement protein attachment,  
344 consequent cytokine liberation and immune cell activation, and the materials do not represent  
345 immediate harm for the cell and/or induce oxidative stress.

## 346 **5. Conclusion**

347 The aim of this study was to evaluate how sol-gel coatings with distinct *in vivo* outcomes  
348 modulate oxidative stress and inflammatory responses. Although there was no differences in  
349 oxidative stress, coatings with low biocompatibility (50M50G and 50V50G) had pro-  
350 inflammatory profiles with higher secretion of TNF- $\alpha$ . Moreover, these materials showed a

351 higher expression of M1 receptors (IL7-R); however, the expression of M2 receptors (CD206)  
352 was not significantly different, indicating that M1 and M2 balance is key to define  
353 inflammatory responses to a biomaterial.

## 354 **6. Acknowledgments**

355 This work was supported by MINECO [MAT MAT2017-86043-R; RTC-2017-6147-1];  
356 Universitat Jaume I [POSDOC/2019/28] and Generalitat Valenciana  
357 [GRISOLIAP/2018/091]. Authors would like to thank Antonio Coso (GMI-Ilerimplant) for  
358 their inestimable contribution to this study, and Raquel Oliver and Jose Ortega for their  
359 valuable technical assistance.

## 360 **7. References**

- 361 1. Anderson JM. Biocompatibility. Polym Sci A Compr Ref 10 Vol Set. Elsevier; 2012.
- 362 2. Anderson JM, McNally AK. Biocompatibility of implants: Lymphocyte/macrophage  
363 interactions. Semin Immunopathol. 2011;33:221–33.
- 364 3. Chen L, Deng H, Cui H, Fang J, Zuo Z, Deng J, Li Y, Wang X, Zhao L. Inflammatory  
365 responses and inflammation-associated diseases in organs. Oncotarget. Impact Journals  
366 LLC; 2018.
- 367 4. Martinez FO. Macrophage activation and polarization. Front Biosci. 2008;13:453.
- 368 5. Anderson JM, Rodriguez A, Chang DT. Foreign body reaction to biomaterials. Semin  
369 Immunol. 2008;20:86–100.
- 370 6. Classen A, Lloberas J, Celada A. Macrophage activation: Classical vs. alternative.  
371 Methods Mol Biol. 2009;531:29–43.
- 372 7. Mantovani A, Sica A, Sozzani S, Allavena P, Vecchi A, Locati M. The chemokine



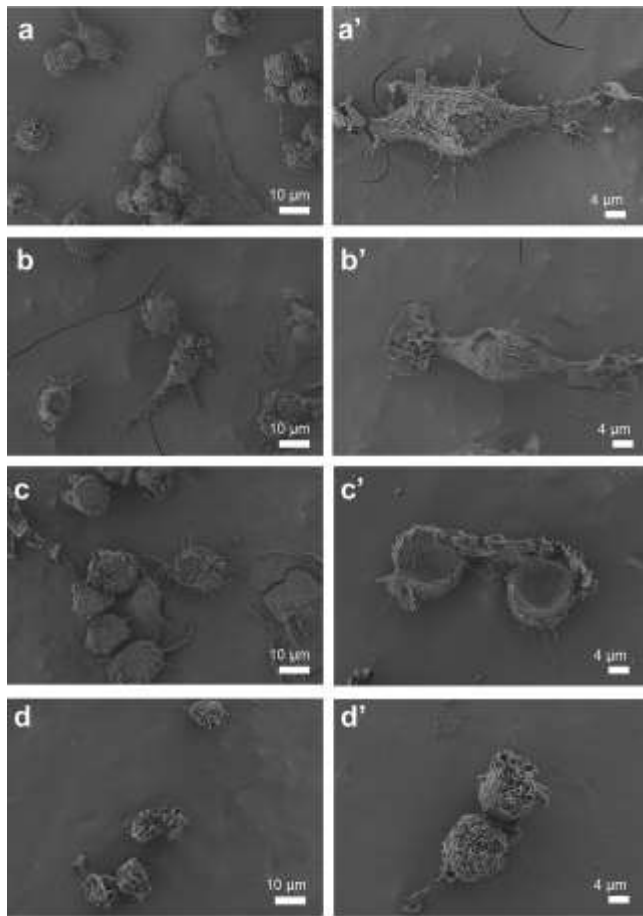
- 373 system in diverse forms of macrophage activation and polarization. *Trends Immunol.*  
374 2004;25:677–86.
- 375 8. Sheikh Z, Brooks PJ, Barzilay O, Fine N, Glogauer M. Macrophages, foreign body  
376 giant cells and their response to implantable biomaterials. *Materials (Basel).*  
377 2015;8:5671–701.
- 378 9. Varin A, Gordon S. Alternative activation of macrophages: Immune function and  
379 cellular biology. *Immunobiology.* Elsevier; 2009;214:630–41.
- 380 10. Brown BN, Londono R, Tottey S, Zhang L, Kukla KA, Wolf MT, Daly KA, Reing JE,  
381 Badylak SF. Macrophage phenotype as a predictor of constructive remodeling  
382 following the implantation of biologically derived surgical mesh materials. *Acta*  
383 *Biomater. Acta Materialia Inc.;* 2012;8:978–87.
- 384 11. Thomsen P, Gretzer C. Macrophage interactions with modified material surfaces. *Curr*  
385 *Opin Solid State Mater Sci.* 2001;5:163–76.
- 386 12. Krifka S, Spagnuolo G, Schmalz G, Schweikl H. A review of adaptive mechanisms in  
387 cell responses towards oxidative stress caused by dental resin monomers. *Biomaterials.*  
388 Elsevier; 2013.
- 389 13. Wang F, Zhang S, Vuckovic I, Jeon R, Lerman A, Folmes CD, Dzeja PP, Herrmann J.  
390 Glycolytic Stimulation Is Not a Requirement for M2 Macrophage Differentiation. *Cell*  
391 *Metab. Cell Press;* 2018;28:463-475.e4.
- 392 14. Araújo-Gomes N, Romero-Gavilán F, Sanchez-Pérez AM, Gurruchaga M, Azkargorta  
393 M, Elortza F, Martínez-Ibáñez M, Iloro I, Suay J, Goñi I. Characterization of serum  
394 proteins attached to distinct sol – gel hybrid surfaces. 2017;1–9.
- 395 15. Sridharan R, Cameron AR, Kelly DJ, Kearney CJ, O’Brien FJ. Biomaterial based

- 396 modulation of macrophage polarization: A review and suggested design principles.  
397 Mater Today. Elsevier Ltd.; 2015;18:313–25.
- 398 16. Romero-Gavilán F, Sanchez-Pérez AM, Araújo-Gomes N, Azkargorta M, Iloro I,  
399 Elortza F, Gurruchaga M, Goñi I, Suay J. Proteomic analysis of silica hybrid sol-gel  
400 coatings: a potential tool for predicting the biocompatibility of implants in vivo.  
401 Biofouling. 2017;33:676–89.
- 402 17. Araújo-Gomes N, Romero-Gavilán F, García-Arnáez I, Martínez-Ramos C, Sánchez-  
403 Pérez AM, Azkargorta M, Elortza F, de Llano JJM, Gurruchaga M, Goñi I, Suay J.  
404 Osseointegration mechanisms: a proteomic approach. J Biol Inorg Chem. Springer  
405 Berlin Heidelberg; 2018;23:459–70.
- 406 18. Romero-Gavilán F, Araújo-Gomes N, Sánchez-Pérez AM, García-Arnáez I, Elortza F,  
407 Azkargorta M, de Llano JJM, Carda C, Gurruchaga M, Suay J, Goñi I. Bioactive  
408 potential of silica coatings and its effect on the adhesion of proteins to titanium  
409 implants. Colloids Surfaces B Biointerfaces. 2017;162:316–25.
- 410 19. Romero-Gavilán F, Gomes NC, Ródenas J, Sánchez A, , Mikel Azkargorta, Ibon Iloro  
411 F, Elortza IGA, Gurruchaga M, Goñi I, Suay and J. Proteome analysis of human serum  
412 proteins adsorbed onto different titanium surfaces used in dental implants. Biofouling.  
413 2017;33:98–111.
- 414 20. Reed DJ, Babson JR, Beatty PW, Brodie AE, Ellis WW, Potter DW. High-performance  
415 liquid chromatography analysis of nanomole levels of glutathione, glutathione  
416 disulfide, and related thiols and disulfides. Anal Biochem. Academic Press;  
417 1980;106:55–62.
- 418 21. Richard A. Lawrence, Parkhill LK, Burk RF. Hepatic Cytosolic Non Selenium-

- 419 Dependent Glutathione Peroxidase Activity: Its Nature and the Effect of Selenium  
420 Deficiency. *J Nutr.* 1978;108:981–987.
- 421 22. Smith IK, Vierheller TL, Thorne CA. Assay of glutathione reductase in crude tissue  
422 homogenates using 5,5'-dithiobis(2-nitrobenzoic acid). *Anal Biochem.* Academic  
423 Press; 1988;175:408–13.
- 424 23. Richard MJ, Guiraud P, Meo J, Favier A. High-performance liquid chromatographic  
425 separation of malondialdehyde-thiobarbituric acid adduct in biological materials  
426 (plasma and human cells) using a commercially available reagent. *J Chromatogr B*  
427 *Biomed Sci Appl.* Elsevier; 1992;577:9–18.
- 428 24. Romero FJ, Bosch-Morell F, Romero MJ, Jareño EJ, Romero B, Marín N, Romá J.  
429 Lipid peroxidation products and antioxidants in human disease. *Environ Health*  
430 *Perspect.* 1998;106:1229–34.
- 431 25. Romero-Gavilán F, Araújo-Gomes N, Cerqueira A, García-Arnáez I, Martínez-Ramos  
432 C, Azkargorta M, Iloro I, Gurruchaga M, Suay J, Goñi I. Proteomic analysis of  
433 calcium-enriched sol–gel biomaterials. *JBIC J Biol Inorg Chem.* Springer Berlin  
434 Heidelberg; 2019;24:563–74.
- 435 26. Araújo-Gomes N, Romero-Gavilán F, Zhang Y, Martinez-Ramos C, Elortza F,  
436 Azkargorta M, Martín de Llano JJ, Gurruchaga M, Goñi I, van den Beucken JJJP, Suay  
437 J. Complement proteins regulating macrophage polarisation on biomaterials. *Colloids*  
438 *Surfaces B Biointerfaces.* Elsevier; 2019;181:125–33.
- 439 27. McWhorter FY, Wang T, Nguyen P, Chung T, Liu WF. Modulation of macrophage  
440 phenotype by cell shape. *Proc Natl Acad Sci.* 2013;110:17253–8.
- 441 28. Jia Y, Yang W, Zhang K, Qiu S, Xu J, Wang C, Chai Y. Nanofiber arrangement

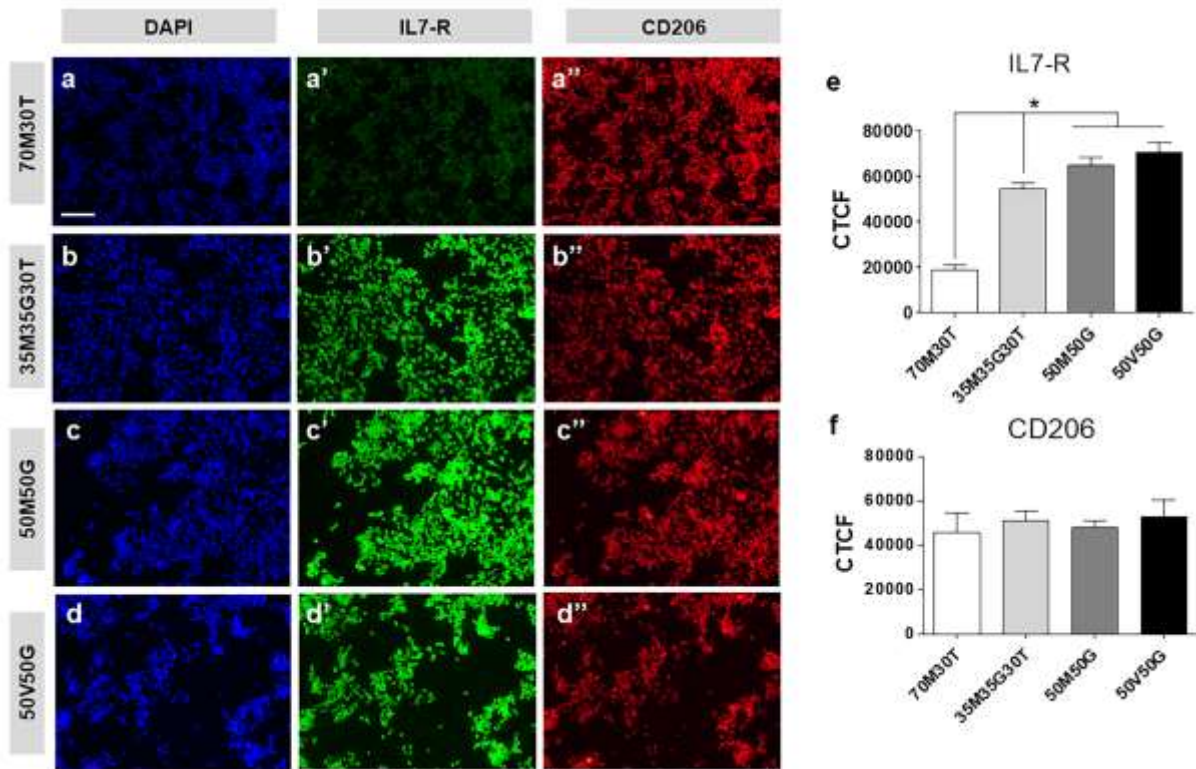
- 442 regulates peripheral nerve regeneration through differential modulation of macrophage  
443 phenotypes. *Acta Biomater. Acta Materialia Inc*; 2019;83:291–301.
- 444 29. Gu Q, Yang H, Shi Q. Macrophages and bone inflammation. *J Orthop Transl.*  
445 Elsevier Ltd; 2017;10:86–93.
- 446 30. Spiller KL, Nassiri S, Witherel CE, Anfang RR, Ng J, Nakazawa KR, Yu T, Vunjak-  
447 Novakovic G. Sequential delivery of immunomodulatory cytokines to facilitate the  
448 M1-to-M2 transition of macrophages and enhance vascularization of bone scaffolds.  
449 *Biomaterials.* Elsevier Ltd; 2015;37:194–207.
- 450 31. Pengal RA, Ganesan LP, Wei G, Fang H, Ostrowski MC, Tridandapani S.  
451 Lipopolysaccharide-induced production of interleukin-10 is promoted by the  
452 serine/threonine kinase Akt. *Mol Immunol.* Pergamon; 2006;43:1557–64.
- 453 32. Anders LC, Lang AL, Anwar-Mohamed A, Douglas AN, Bushau AM, Falkner KC,  
454 Hill BG, Warner NL, Arteel GE, Cave M, McClain CJ, Beier JJ. Vinyl Chloride  
455 Metabolites Potentiate Inflammatory Liver Injury Caused by LPS in Mice. *Toxicol Sci.*  
456 2016;151:312–23.
- 457 33. Veremeyko T, Yung AWY, Anthony DC, Strekalova T, Ponomarev ED. Early Growth  
458 Response Gene-2 Is Essential for M1 and M2 Macrophage Activation and Plasticity by  
459 Modulation of the Transcription Factor CEBP $\beta$ . *Front Immunol.* Frontiers Media S.A.;  
460 2018;9:2515.
- 461 34. Li S, Miao T, Sebastian M, Bhullar P, Ghaffari E, Liu M, Symonds ALJ, Wang P. The  
462 Transcription Factors Egr2 and Egr3 Are Essential for the Control of Inflammation and  
463 Antigen-Induced Proliferation of B and T Cells. *Immunity.* 2012;37:685–96.

464



466

467 **Figure 1.** Cell morphological analysis by SEM. Sample microphotographs of RAW 264.7  
468 cultured on (a-a') 70M30T, (b-b') 35M35G30T, (c-c') 50M50G, (d-d') and 50V50G sol-gel  
469 hybrid coatings after 72h. Scale bar: 10  $\mu\text{m}$  and 4  $\mu\text{m}$ .



470

471 **Figure 2.** Immunostaining of RAW264.7 cells cultured on (a-a'') 70M30T, (b-b'')

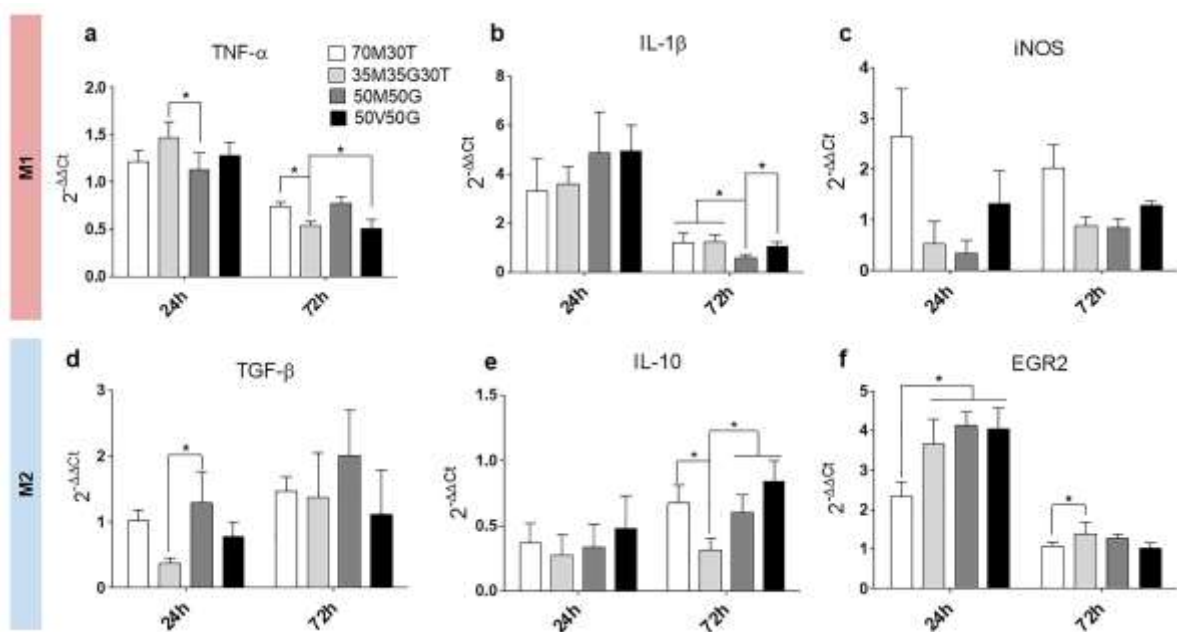
472 35M35G30T, (c-c'') 50M50G, and (d-d'') 50V50G sol-gel hybrid coatings, after 72h. IL7-R

473 (a'-d') was used as a M1 marker and CD206 (a''-d'') was used as a M2 marker. The relative

474 corrected total cell fluorescence (CTCF) of these markers (e and f) was quantified using

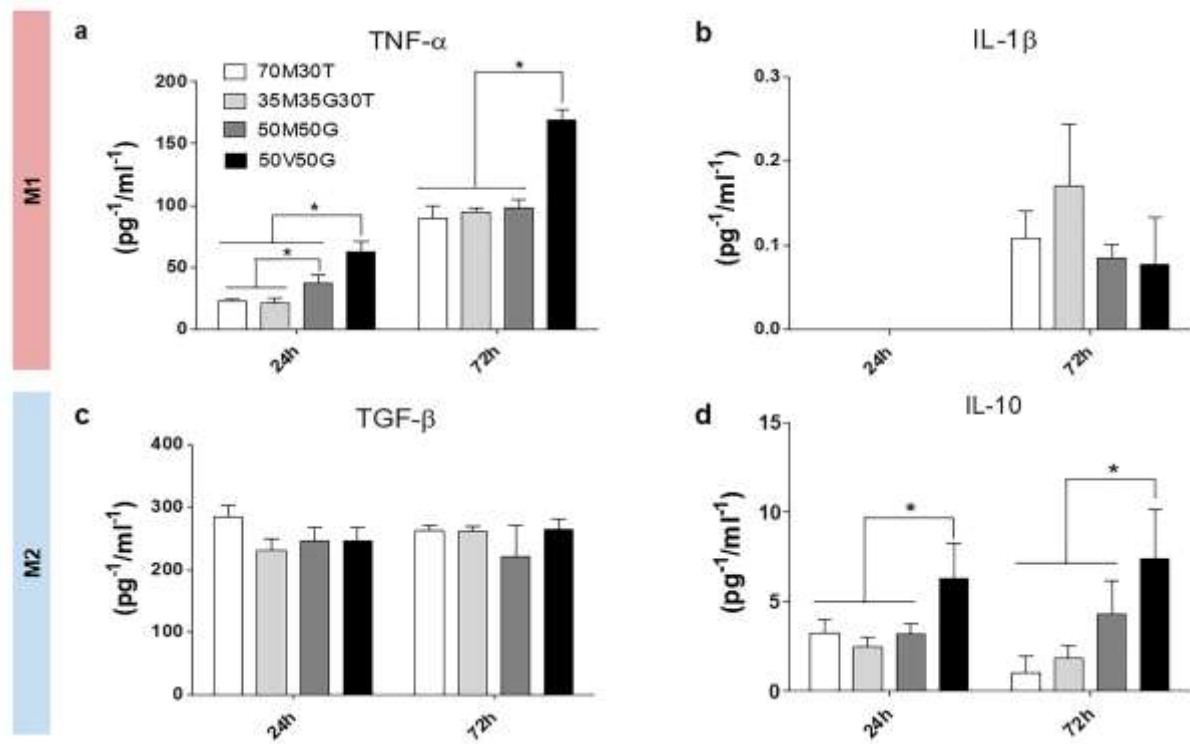
475 ImageJ. Data are presented as mean  $\pm$  SD. The asterisk (\*) indicates differences between

476 materials ( $p < 0.05$ ). Scale bar: 100 $\mu$ m.



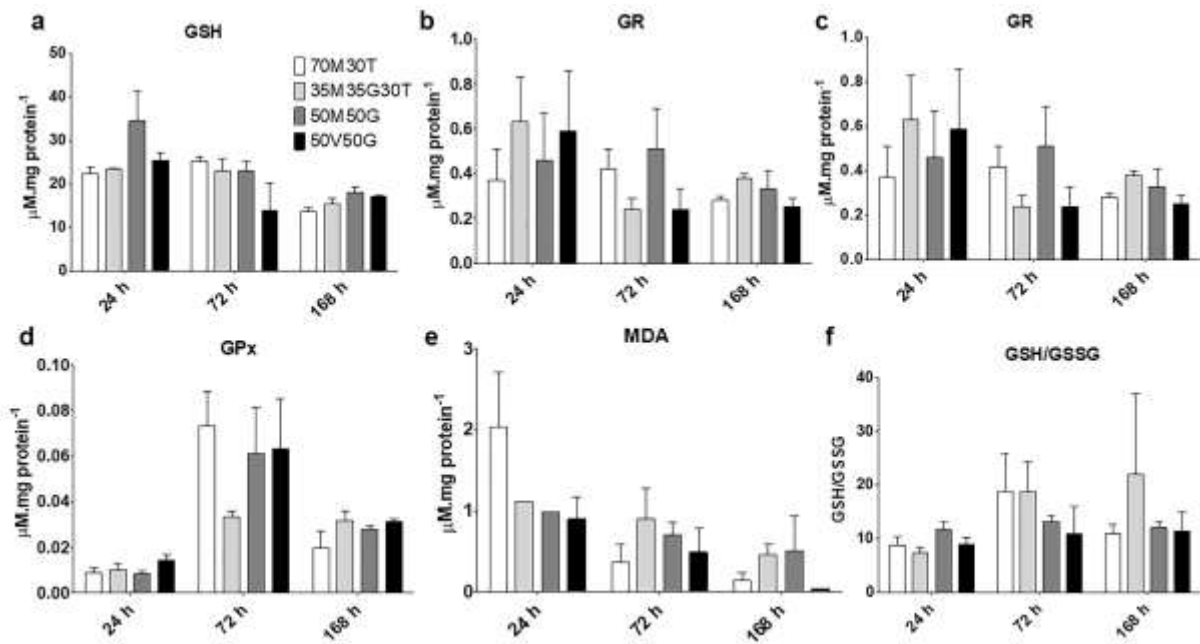
477

478 **Figure 3.** Gene expression of RAW264.7 cells cultured on 70M30T, 35M35G30T, 50M50G  
 479 and 50V50G on the sol-gel hybrid coatings after 24 and 72h: (a) TNF- $\alpha$  (a), (b) IL-1 $\beta$ , (c)  
 480 iNOS, (d) TGF- $\beta$ , (e) IL10, and (f) EGR2. Data were normalized to blank wells (without  
 481 material) and are presented as mean  $\pm$  SD. The asterisk (\*) indicates differences between  
 482 materials ( $p < 0.05$ ).



483

484 **Figure 4.** Cytokine secretion of RAW264.7 cells cultured on 70M30T, 35M35G30T,  
 485 50M50G and 50V50G on the sol-gel hybrid coatings after 24 and 72h: (a) TNF- $\alpha$ , (b) IL1- $\beta$ ,  
 486 (c) TGF- $\beta$ , and (d) IL-10. Data are presented as mean  $\pm$  SD. The asterisk (\*) indicates  
 487 differences between materials ( $p < 0.05$ ).



488

489 **Figure 5.** Oxidative stress markers of RAW264.7 cells cultured on 70M30T, 35M35G30T,  
 490 50M50G and 50V50G on the sol-gel hybrid coatings after 24, 72 and 168h: (a) GSH, (b)  
 491 GSSG, (c) GR, (d) GPx, (e) MDA, (f) GSH/GSSG. Results are shown as mean  $\pm$  SD.